Boundary layer and aerosol evolution during the 3rd Lagrangian experiment of ACE-2

By ROBERT WOOD[1]*, DOUG JOHNSON[1], SIMON OSBORNE[1], MEINRAT O. ANDREAE[2], BRIAN BANDY[3], TIMOTHY S. BATES[4], COLIN O'DOWD[5], PAUL GLANTZ[6], KEVIN NOONE[6], PATRICIA K. QUINN[4], JOCHEN RUDOLPH[7] and KARSTEN SUHRE[8], [1]*Meteorological Research Flight, Meteorological Office, Farnborough, UK;* [2]*Biogeochemistry Department, Max Planck Institute, Mainz, Germany;* [3]*School of Environmental Sciences, University of East Anglia, Norwich, UK;* [4]*NOAA/PMEL, Seattle, USA;* [5]*Centre for Marine and Atmospheric Science, University of Sunderland, UK;* [6]*Department of Meteorology, University of Stockholm, Sweden;* [7]*Centre for Atmospheric Chemistry, York University, Canada;* [8]*Laboratoire d'Aerologie, Toulouse, France*

ABSTRACT

Aircraft measurements are presented of the Lagrangian evolution of a marine boundary layer over a 30-h period during the ACE-2 field campaign. At the start of the observational period, a 500-m deep polluted marine internal boundary layer (MIBL) was overlain by the remnants of a polluted continental boundary layer extending to around 2 km below a clean, dry free troposphere. The MIBL grew rapidly to a thickness of 900–1000 m in response to increasing sea surface temperatures. No significant aerosol spectral evolution was observed in the boundary layer. Low concentrations of SO_2 were observed in the MIBL suggesting that the air mass contained relatively aged aerosol. Aerosol spectra show a broad mode with a modal diameter of around 0.1 μm. The polluted layer between the MIBL and the unpolluted free troposphere was only weakly and intermittently turbulent which prevented significant entrainment of clean air into the polluted layer from aloft. The polluted layer depth was thus controlled mainly by subsidence which as a result becomes shallower, decreasing from over 2000 m to around 1200 m during the observational period. The aerosol characteristics of the polluted layer were similar to those in the MIBL and so although the MIBL entrained considerable amounts of air from above the MIBL the aerosol characteristics underwent no significant change. This has important implications for the rate at which a polluted continental air mass is converted to a clean marine one. The dataset should prove useful in the validation of the modelling of continental pollution outbreaks.

1. Introduction

Considerable interest is currently being focused upon the distribution of both natural and anthro-

pogenic aerosol over the ocean (Bates et al., 1998; VanDingenen et al., 1999). The 2nd Aerosol Characterisation Experiment (ACE-2) intensive observational period and associated ongoing observational campaigns (Raes et al., 2000) were designed with the long-term goal being a better understanding of the radiative effects of anthropogenically produced atmospheric aerosol in the North Atlantic region. Large variations in aerosol characteristics are observed in this region due to

---

* Corresponding author address: Meteorological Research Flight, Building Y46, DERA, Farnborough, Hampshire, GU14 0LX, UK.
e-mail: robwood@meto.gov.uk.

the frequent continental outbreaks which advect highly polluted air from continental Europe into an otherwise relatively clean background. Understanding the processes associated with the transport and evolution of aerosol advected from continental source regions is fundamental in the quest to determine the overall radiative forcing in the region (ACE-2 Science and Implementation Plan, IGAC, April 1995). The ACE-2 Lagrangian experiments (Johnson et al., 2000) were designed to follow marine boundary layer air mass trajectories and to determine the physical and chemical processes important in aerosol evolution over the ocean.

A range of processes are thought to have important effects upon the evolution of polluted aerosol. A summary of these effects together with estimates for their importance can be found in Van Dingenen et al. (1999) which concludes that entrainment of free tropospheric air into the boundary layer is the single most important process controlling the relationship between the total sulphate mass and the number of aerosol which can be activated to form cloud droplets after the polluted air is advected away from the source over the sea. The processes of coagulation, precipitation, condensation and in-cloud oxidation are found, given the simple physical parameterisations used in the study, to be significantly less important than entrainment. In this modelling study, the pollution was all contained within the marine boundary layer. Continental boundary layers, especially during the summer months, are often considerably higher than those found over the oceans at similar latitudes due to the typically larger surface heat fluxes. Over land, close to the source region, pollution can thus be expected to reach considerable altitudes. If this air is advected over the ocean then surface fluxes over the ocean cannot usually support such a deep boundary layer and a shallower marine internal boundary layer (MIBL) will grow within the continental one (Stull, 1988). In this case the lower troposphere will exhibit quite a complicated structure with remnants of humid convective boundary layers overlying freshly-grown marine internal boundary layers.

The Lagrangian approach centres upon the repeated measurement of an air mass over an extended period to observe changes in parameters of interest. Only with this technique is it possible to study time-dependent processes with some confidence. Although there are some major advantages to the adoption of a Lagrangian approach, there are some caveats: (i) trajectories for different levels in the lower troposphere may well be different due to differential advection between levels. This means that only observations at one level can be considered to be truly of a Lagrangian nature. (ii) the Lagrangian approach is only truly applicable to homogeneous air masses without strong horizontal gradients. More discussion of the Lagrangian experimental concept can be found in Businger et al. (1999) and Russell et al. (1998).

To date, little work has been carried out to examine the vertical structure and evolution of aerosol in lower-tropospheric multi-layered continental outbreaks over the ocean. In this paper observational details are presented of the evolution of a polluted air mass as it is advected over the Atlantic Ocean north of the Canary Islands. A brief description of the flights is presented and the air mass origins are discussed in Section 2. Instrumentation is briefly discussed in Section 3. Observational results are presented in Sections 4 and 5, with the former being a discussion of the general layer structure and the latter describing results describing each layer and its evolution in more detail. Much of the general overview of the experiment can be found in Johnson et al. (2000). The final section includes a brief summary of the important results and the conclusions to be drawn therefrom, summarising the most important findings in the form of hypotheses pertaining to continental pollution outbreaks that are worthy of further investigation by process modellers.

2. Description of flights and air mass origins

A general description of the flights, the flight tracks and sampling methods can be found in the Lagrangian experiments summary paper (Johnson et al., 2000). Three flights were used to characterise the boundary layer and lower free troposphere during a 30-h period from approximately 1100 UTC 23 July 1997 to 1700 UTC 24 July 1998. Table 1 shows the approximate times and locations at which measurements were being made in the Lagrangian air parcel. The position of the observational air mass was defined by the position

Table 1. *Flight details for Lagrangian 3*

Flight no.	Start time (UTC)	End time (UTC)	Start pos. (°N; °W)	End pos. (°N; °W)
A566	1130	1600	38.2; 12.5	37.0; 12.0
A567	2230	0500	35.1; 11.1	33.5; 11.1
A568	1000	1700	31.8; 12.1	30.2; 13.3

The start and end times refer to C-130 observations in the Lanrangian air mass. The start and end positions give the approximate positions of the centre of the box.

of a smart balloon (Johnson and Businger, 2000) launched from the research vessel RV Vodyanitsky at 0730 UTC 23 July at a position approximately 40°N, 12°30′W. A PFC tracer released at the same time as the balloon also provided confidence that the aircraft was sampling the same air mass throughout the experment. A more complete description of the aircraft sampling strategy is given in Johnson et al. (2000).

The origins of the air mass observed in Lagrangian 3 are investigated using air mass back trajectories which are described in some detail by Johnson et al. (2000). Back trajectories were calculated from ECMWF data using a code developed by Draxler and Hess. (1997). These show that the observed air mass can be traced back to a highly polluted region of continental Europe (Fig. 1). The air mass was over the ocean for 2 days prior to the start of the observational period of Lagrangian 3 after leaving the continent in the vicinity of the Bay of Biscay.

3. Instrumentation

A more complete overview of the instrumentation used during the Lagrangian experiments is found in Johnson et al. (2000). A brief description is given in this section.

3.1. Turbulence, thermodynamics, SST

Turbulent parameters discussed in this paper were calculated using an eddy-correlation method from high-frequency wind, temperature and moisture data. Each time series was linearly detrended and then a moving average high-pass filter was applied with a width of 50 s (equivalent to a spatial

length scale of approximately 5 km). This technique removes mesoscale features and potential errors caused by instrumental drift. Sea surface temperature was measured using a Heimann KT19 nadir-viewing radiometer on the C-130. Corrections for atmospheric absorption between the aircraft and the sea surface have been applied. Using an observed profile from close to the sea surface up to a height of over 5 km and assimilating this to a mid-latitude summertime profile above this height estimates of the corrections required to correct the observed SST for reflection of clear sky radiance were obtained (Hignett, 1998). These suggest that in cloud-free conditions the correction from reflectance of clear sky is 0.5–0.65 K using the sea water emissivity of Masuda et al. (1988).

3.2. Aerosol and chemistry measurements

In this paper, dry aerosol size distributions are measured using a differential mobility analyser (0.01–0.25 μm) and a PCASP (0.1–3.0 μm). Further information on aerosol concentration is available from a condensation nucleus counter (CNC-3025) which provides total aerosol concentration for particles larger than 0.003 μm. Chemical composition is obtained using filter samples. Stainless steel cannister samples obtained at different heights during Lagrangian 3 were analysed for non-methane hydrocarbons (NMHC). Ozone was measured using a commercial TECO 49 instrument. More details on the instrumentation are presented in Johnson et al. (2000).

4. Vertical lower-tropospheric structure

4.1. General overview

This section is intended to give a general overview of the layer structure and its evolution over the course of the observational period. More detailed analyses of the different layers and their interaction is presented in the following sections.

Considerable changes in the structure of the lower troposphere were observed during the experiment. Fig. 2 shows a schematic diagram of the lower-tropospheric evolution during the 30-h hour period in which aircraft observations were made. The main dynamical feature is the presence
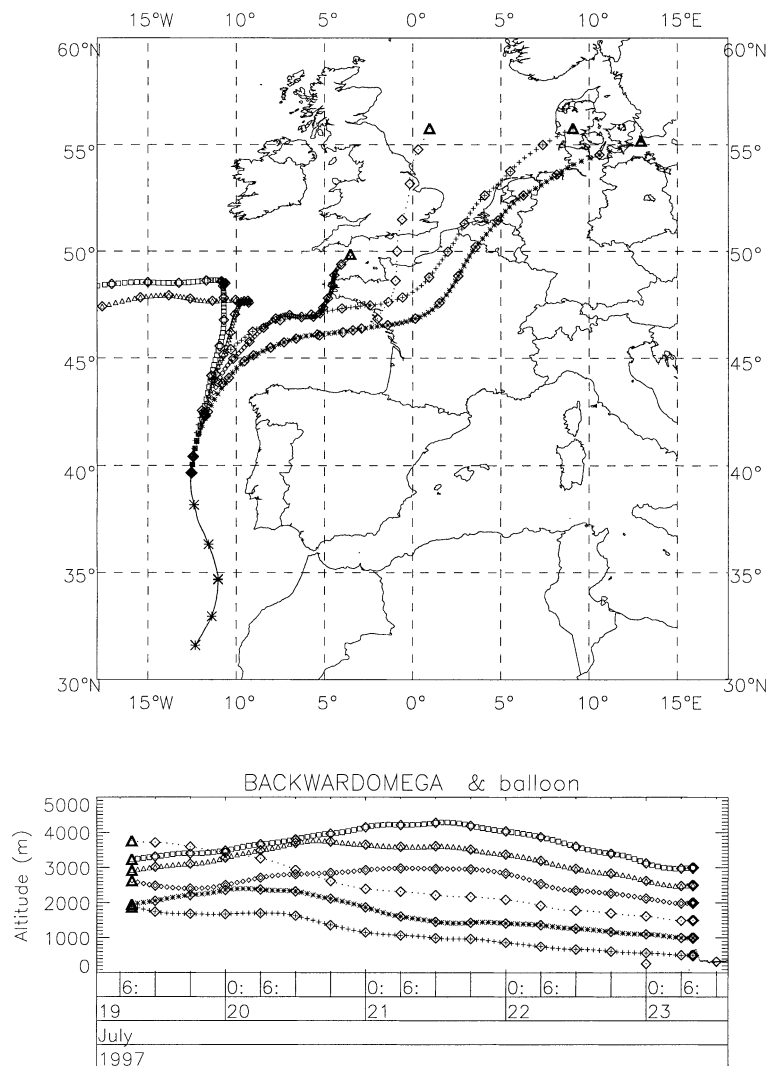
Fig. 1. Back trajectory analysis for air at 6 different heights (500–3000 m) at the time of the balloon release marking the start of Lagrangian 3. The upper panel shows the horizontal position of the air parcels and the lower panel the height of the trajectories.

of a marine internal boundary layer which deepened considerably during the observational period. During the 1st and the 3rd flights little change in the boundary layer thermodynamic and dynamic structure was observed. However, during the 2nd flight the boundary layer deepened from around 450–550 m to 900–950 m. On the 1st flight (A566), small amounts of weak cumulus humilis cloud (bases 300 m; tops 450–500 m) were present beneath the MIBL inversion. At the beginning of

this flight at around midday the cloud was observed to form in quasi-linear structures aligned roughly parallel to the mean wind speed. This suggests that some of the turbulent transfer was achieved through boundary layer rolls (Brooks and Rogers, 1997). By the end of flight 1 the cumulus cloud cover had increased substantially (although no significant increase in the MIBL depth was observed) and no roll-like structures were observed. At the start of the second flight
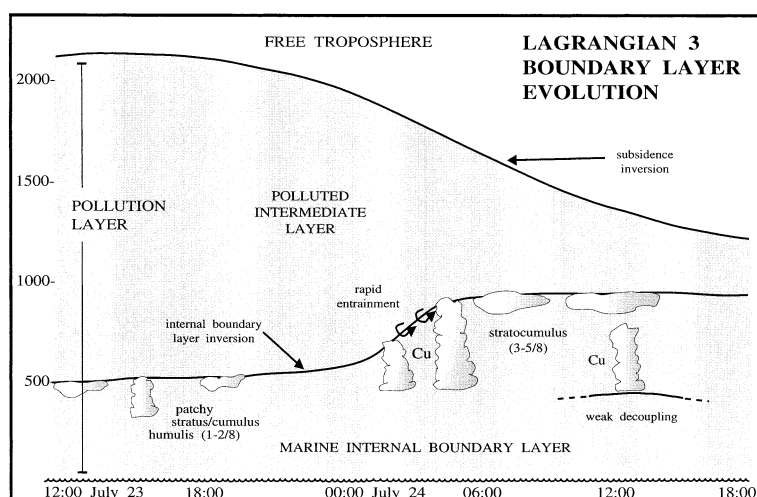
Fig. 2. Schematic diagram of lower-tropospheric evolution during ACE-2 Lagrangian experiment 3. A shallow marine internal boundary layer (MIBL) deepens as aresponse to increasing sea surface temperatures. Above the MIBL a moist layer extends initially up to 2000 m and serves as a buffer layer between the internal boundary layer and the free troposphere above. The buffer layer becomes shallower during the observational period due to subsidence and the fact that only weak turbulence levels prevent considerable growth of the layer through entrainment. Both the MIBL and the buffer layer are polluted which suggests that the buffer layer is a remnant of a once continental boundary layer in which vertical mixing carried pollution to an altitude of at least 2 km. Periods of observation are shown by horizontal bars.

(A567), cumulus clouds were again observed (bases 300 m; tops 500–700 m). During the flight the cumulus clouds grew significantly with a rapid simultaneous deepening of the MIBL. By the end of the flight the MIBL was around 900–950 m. No significant further increase in the depth of the MIBL took place in the time between the end of flight 2 and the start of flight 3 (approximately 5 h). At the start of flight 3 (A568) the MIBL was capped by broken stratocumulus cloud with cumulus clouds present below. The MIBL exhibited weak decoupling which persisted throughout the 3rd flight. The stratocumulus fractional cloud coverage was greatest at the start of flight 3 and had become considerably more broken by the end of the flight. The MIBL depth stayed roughly constant (900–1000 m) during the flight.

The schematic diagram of boundary layer evolution (Fig. 2) indicates the presence of a reasonably homogeneous polluted layer extending up to a subsidence inversion at a height of more than 2000 m at the start of the observational period. That the pollution is not simply confined to the marine internal boundary layer suggests that the layer between the top of the MIBL and the

subsidence inversion was once part of a well-mixed boundary layer (no frontal activity was encountered by the air during advection over the ocean) and that this boundary layer probably formed over the land surface before advection carried the air mass over the ocean. The upper layer has a moisture content lower than that of the MIBL and greater than that of the free tropospheric air just above the subsidence inversion.

4.2. Inversion heights

Fig. 3 shows the observations of the heights of the MIBL (triangles) and the subsidence inversion (crosses) during the period of the experiment. These data were obtained from profiles and from short climbs between the box-pattern measurement levels. Sharp jumps in total water content q_T were associated with all the inversions, and the inversion heights shown here are defined as the height at which the total water content is equal to the mean of the total water contents in the two layers adjacent to the inversion. Different definitions of the inversion height (e.g., those based upon turbulence mixing heights or potential
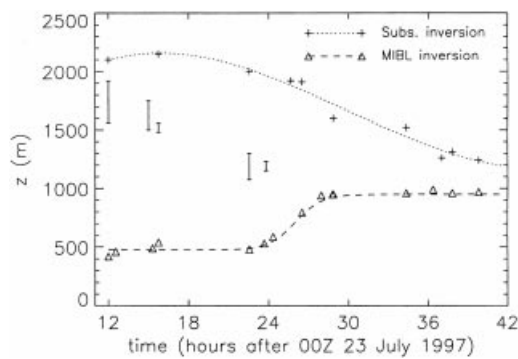
Fig. 3. Inversion heights during Lagrangian 3 observed using the C-130 aircraft. The symbols are: MIBL inversion (triangles); subsidence inversion (crosses). The dashed and dotted lines represent fits to the observational data. Profiles prior to 0000 UTC 24 July show a dry layer within the otherwise relatively homogeneous layer below the subsidence inversion and the vertical extent of this layer is marked by the vertical bars.

temperature) were found to give inversion heights that differed from those presented by less than 50 m. The dashed and dotted lines in Fig. 3 show curve-fits to the MIBL inversion height (z_i) and the subsidence inversion height (z_{subs}) respectively. More details and the application to the study of entrainment rates is presented in Solazzo et al. (2000).

The vertical bars show the vertical extent of a clean, dry layer that had probably moved into the polluted air column as a result of differential advection. This conclusion is supported by the fact that aerosol concentrations and spectra above and below this clean layer are very similar apart from during the initial stages of the the 1st flight where the separated pollution layers appear to be quite distinct in origin. The observed thickness of this clean layer shows considerable variability and this is more likely a result of spatial variability than temporal variability. The dry layer was not observed at all after 0000 UTC 24 June.

4.3. Vertical thermodynamic structure

Fig. 4 shows the evolution of virtual potential temperature, and specific humidity, from the 1st and the 3rd flights (A566 and A568) during Lagrangian 3. Each plotted point represents an average from a single 7 min (approx 42 km) straight and level run, four of which make up a single box pattern. Also shown are data from single profiles taken at the start of the 1st flight and at the end of the final flight. The horizontal dotted lines separate the different layers. Fig. 4 clearly shows the presence of a low-level moist boundary layer ($q_T > 10\,\mathrm{g\,kg^{-1}}$) which grows during the observational period. Above the MIBL there was a layer with fairly constant humidity intermediate between that of the MIBL and the free troposphere ($q_T \approx 7\,\mathrm{g\,kg^{-1}}$). In this paper the intermediate layer is termed the pollution layer (PL). During the 1st flight (A566) the PL was existed as two distinct polluted layers (PL and UPL) between which a dry layer (DL) was present. Both the PL and the UPL have similar humidities. The depth of the dry layer was variable but was typically 50–350 m deep with its base initially at a height of around 1500 m. Profiles after 24 UTC 23 July show no evidence of a dry layer between two layers of pollution and the top of the polluted layer has subsided considerably. The MIBL, in contrast, has grown to a height of almost 1000 m. The free tropospheric air has warmed substantially due to subsidence warming and the PL has become more statically stable. The jump in virtual potential temperature across the inversion capping the MIBL has also increased in magnitude.

At the start of the 1st flight the wind speed and direction at the lowest aircraft level (120 m) was approximately 10 m s^{-1}/160° (where the direction is given as the direction in which the air is moving rather than from where it has originated). There was some vertical shear with the wind above the MIBL moving in a direction closer to 180°. The shear becomes less pronounced during the second flight with all levels moving with a wind speed and direction of approximately 8–9 m s^{-1}/180°. During the 3rd flight some directional shear was present with the upper level air moving in a direction of around 215° and the MIBL air moving in a direction closer to 200°. The wind speed has also increased to 10–11 m s^{-1} during the 3rd flight.

Fig. 4. Run-mean values and representative profiles of total water content (left) and virtual potential temperature (right) from the 1st (top) and last (bottom) flights. The MIBL grown markedly in height. The vertical extent of the pollution is reduced during the experiment by subsidence. The presence of a dry layer within the polluted layer is observed towards the start of the experiment. There is evidence to suggest that the pollution in the upper polluted layer (UPL) is of different origin to the pollution lower down (see Subsection 4.4.2).
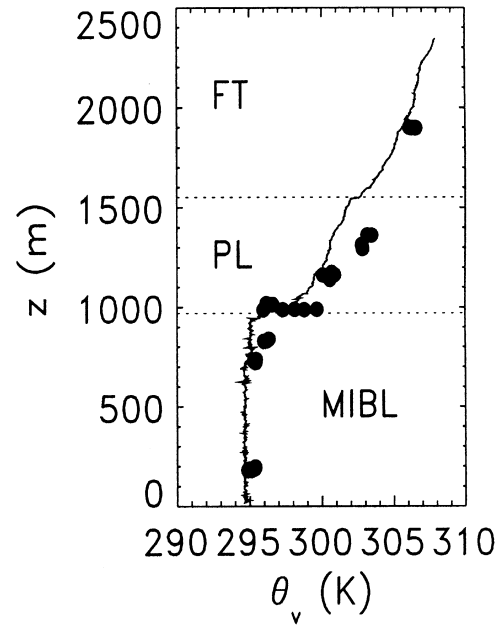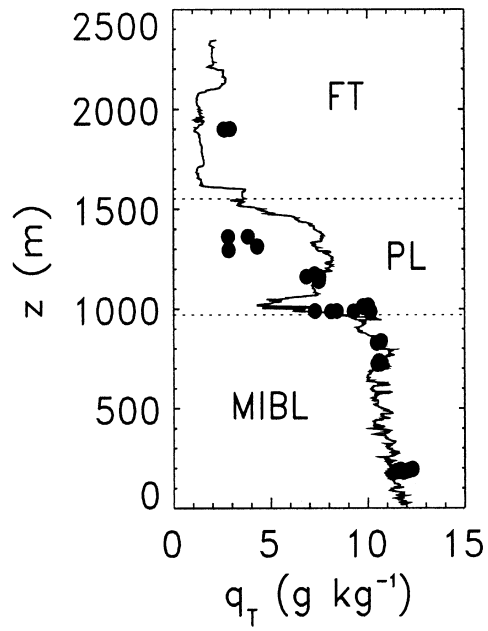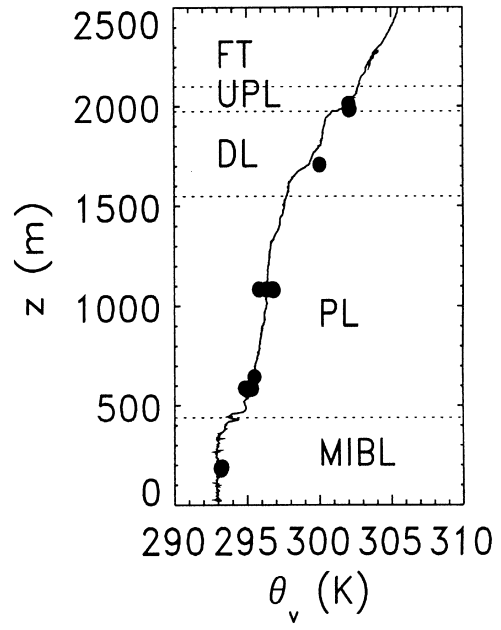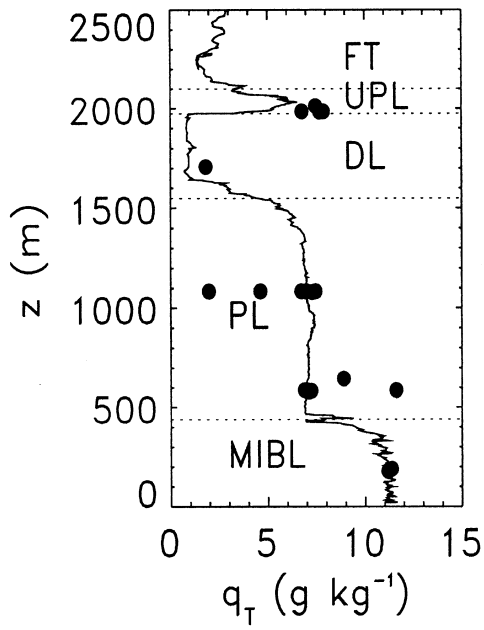
4.4. Vertical pollution structure

4.4.1. Profiles. Fig. 5 shows the total aerosol and accumulation-mode aerosol with $D > 0.1\mu m$ (taken from the wing-mounted PCASP) from two profiles (as in Fig. 4) during Lagrangian 3. The upper plots are taken from a profile at the start of the observational period (12 UTC 23 July). The total aerosol and the accumulation-mode aerosol are highly correlated marking a vertically stratified pollution structure that corresponds to the layers shown in Fig. 4. For example, the drylayer (DL) is also a relatively clean layer with a total aerosol concentration of only 500 cm^{-3}. The upper pollution layer (UPL) is not observed on subsequent profiles. There is a difference in wind velocity between the MIBL and 2000 m in the 1st flight of approximately $2 \text{ m s}^{-1}/10°$. The lack of evidence for the persistence of the upper pollution layer and dry layer in the later flight does not necessarily imply that their identities have been lost by turbulent mixing. Profiles on the 2nd flight (2330 UTC 23 July) (not shown) reveal that the main pollution layer (PL) has seemingly grown in height to just less than 2000 m (Fig. 3). It is unlikely that the turbulence at the top of the pollution layer could have generated entrainment rates large enough to raise the pollution layer depth by almost 500 m. It is more likely that the wind velocity differential between the MIBL and 1500–2000 m has resulted in these apparent changes in vertical structure.

The lower two plots in Fig. 5 show the vertical aerosol structure at 1015 UTC on 24 July. Accumulation-mode aerosol concentrations in the MIBL fall slightly during the experiment (see also Table 2). The polluted layer has decreased markedly in depth and coincides with the layer of intermediate humidity (as it did on the 1st and 2nd flights). It is interesting that both total and accumulation-mode aerosol concentrations are slightly lower in the MIBL than in the PL. This may simply be a result of inhomogeneity within the air mass as the box-averaged total aerosol concentrations (Table 2) do not show a clear reduction in the MIBL given the variability of the aerosol within the layers. The MIBL accumulation mode aerosol concentrations do however show a small decrease through the experiment.

4.4.2. Size distributions and composition. Fig. 6 shows aerosol dry size distributions from the different layers taken on the 1st flight. All spectra

show a broad mode with a modal diameter of approximately 0.1 µm. Distributions from the MIBL, the PL and the UPL have similar shapes although there are some differences: (i) the MIBL distribution shows a fairly distinct coarse mode resulting from sea-salt production in the MIBL; (ii) the broad mode of the UPL distribution extends to larger sizes (0.3–1.0 µm) than those in both the MIBL and the PL; (iii) higher concentrations of aerosol in the size range 0.03–0.06 µm are found in the PL than anywhere else. The reason for (ii) is likely to be the different origins of the aerosol in the PL and UPL. Back-trajectories (Fig. 1) show the histories of different levels within the air mass at the start of Lagrangian 3. Back trajectories for initial heights of 500 m (crosses), 1000 m (asterisks), 1500 m (dots), 2000 m (small diamonds), 2500 m (triangles) and 3000 m (squares) at the start of Lagrangian 3 are shown. These show that air below 1500 m at the start of Lagrangian 3 passed over highly polluted regions in northern France, the Netherlands and Belgium. These regions produce considerable amounts of ammonia from intensive animal farming. In contrast the upper polluted layers at the start of Lagrangian 3 may have passed over the UK, a source of more industrial pollution such as combustion products, particularly sulphur dioxide. Thus, it is likely that the UPL would have contained aerosol with considerably different size distributions and internal chemistry and filter measurements (presented in Section 5) support this conclusion.

Table 2 gives aerosol concentration characteristics for the three flights. Given that there is considerable uncertainty both in the total aerosol number N_{tot} and the DMA and PCASP concentrations (especially in the overlap region where the majority of particles are found), we can only conclude from Table 2 that high concentrations of nucleation mode aerosol do not appear to be present during Lagrangian 3.

Table 3 details the fine-mode ammonium, sulphate, chloride and nitrate mixing ratios. The dominant fine-mode cation in the pollution layers was ammonium with molar mixing ratios typically between 1300–2200 ppt. The concentrations of other cations such as calcium and magnesium were all below 30 ppt. Sodium and potassium mixing ratios were not available from Lagrangian 3. The dominant anion was sulphate
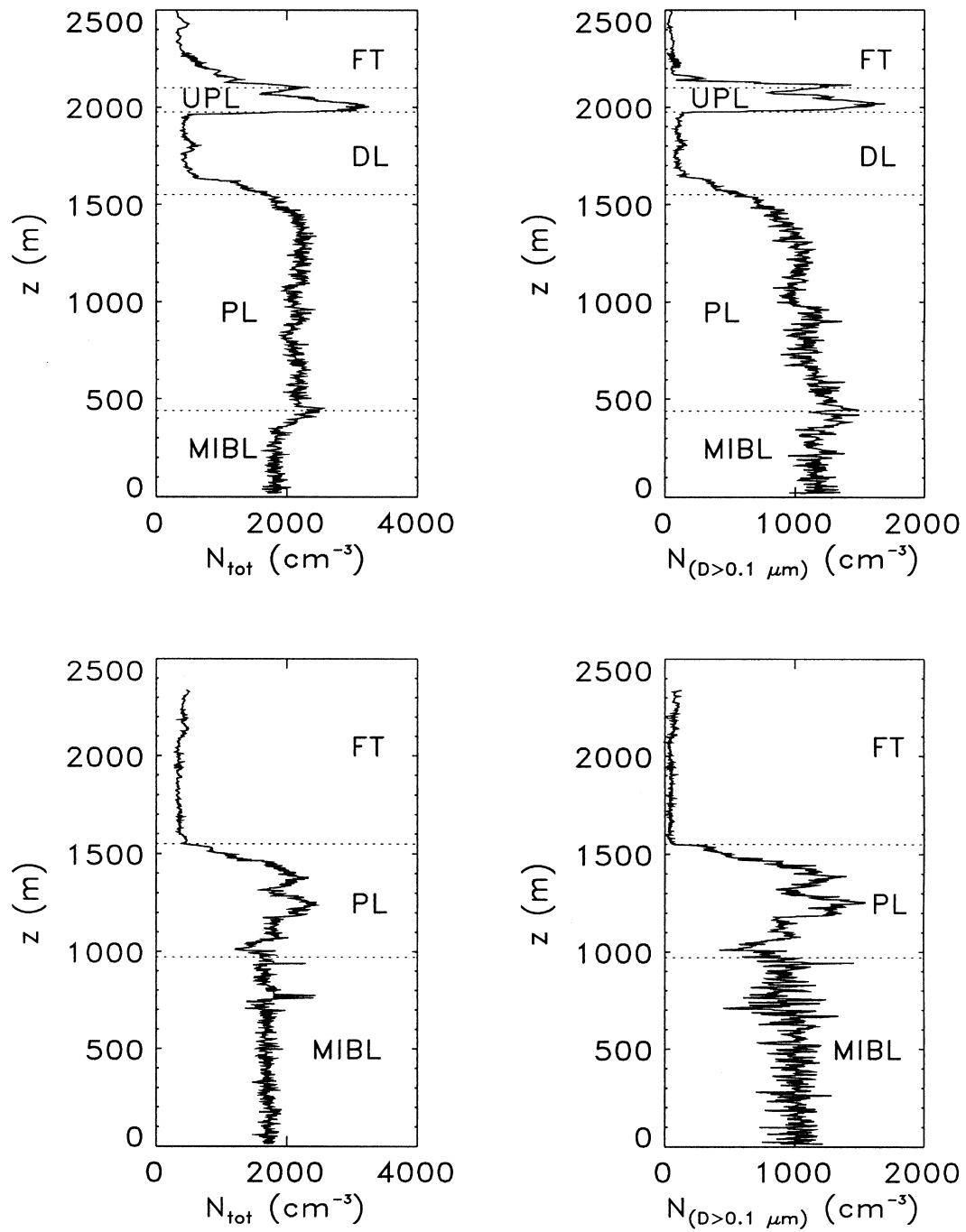
Fig. 5. Representative profiles of total aerosol concentration (left) and concentration of aerosol larger than 0.1 μm (right) from Lagrangian 3. The data are taken from the same profiles shown in Fig. 4.

Table 2. *Aerosol concentrations measured during Lagrangian 3*

Flight, run	z (m)	N_{tot} (cm^{-3})	$N_{PCASP+DMA+FSSP}$ (cm^{-3})	$N_{D>0.1\mu m}$ (cm^{-3})	$N_{D>0.5\mu m}$ (cm^{-3})
		1st flight — 1200–1500 UTC 23 July			
MIBL	120	1730 [130]	1840	1000	3.9
PL	530	2160 [250]	2070	1080	0.6
PL	1040	1970 [170]	1930	950	0.5
DL	1600	674 [110]	690	280	0.2
UPL	1950	2156 [220]	1940	1100	2.0
		2nd flight — 2300 UTC 23 July–0200 UTC 24 July			
MIBL	250	1820 [220]	1700	990	4.2
MIBL	530	1700 [200]	1660	940	—
MIBL	870	1780 [360]	1640	820	—
PL	1370	1850 [120]	1780	890	0.5
FT	2020	400 [50]	320	120	0.2
		3rd flight — 1200–1500 UTC 24 July			
MIBL	120	1690 [100]	1850	920	3.8
MIBL	770	1620 [160]	1750	880	6.9
MIBL	930	1630 [230]	1700	840	0.9
PL	1120	1770 [270]	—	900	0.9
FT	1860	390 [60]	300	60	0.1

A number of size classifications are used: N_{tot} is the total aerosol concentration of aerosol with diameters larger than approximately 0.003 μm; $N_{DMA+PCASP+FSSP}$ is the total concentration in the diameter range 0.01–47.0 μm; $N_{D>0.1\mu m}$ is the concentration in the accumulation size range — soluble aerosol in this size range has the potential to be activated to form cloud droplets; $N_{D>0.5\mu m}$ is the coarse mode concentration. Each tabulated measurement represents the mean over a horizontal box pattern. Figures inside the square brackets are the standard deviations of the total aerosol concentration.

(500–1000 ppt in the polluted layers) followed by chloride (40–230 ppt) and nitrate (20–90 ppt). Table 4 shows the coarse-mode molar mixing ratios for the dominant soluble species. The large aerosol soluble composition was dominated throughout Lagrangian 3 by sodium and chloride in the MIBL, with smaller contributions from ammonium, sulphate, nitrate, calcium, magnesium and potassium. More details of the ionic species within the aerosol are presented in Section 5.

4.4.3. Gas-phase chemistry measurements. Hydrocarbon concentrations (Table 5) are typical for photochemically aged air masses with marginal impact from recent urban or industrial emissions. The hydrocarbon concentrations indicate that the level of anthropogenic impact is somewhat lower in the FT than in the MIBL. On average the highest NMHC mixing ratios are found in the PL and UPL although the differences are often small and not always statistically significant.

Fig. 7 shows profiles of ozone concentration during Lagrangian 3 as a function of time (times

shown at top). Ozone concentrations greater than 60 ppb are plotted using a thicker linestyle to highlight the fact that the ozone concentrations are highest in the polluted layer above the MIBL. The ozone falls above the subsidence inversion and in the MIBL. Also of particular interest is the fact that the ozone concentration in the polluted layer shows no clear decrease with time over the 30 h period of the observations. This suggests that ozone concentrations are in a dynamic equilibrium possibly involving other pollutant species or that destruction rates in the PL are very slow. The reduced concentrations in the MIBL are likely to result from the higher relative humidity which facilitates ozone removal. Dry deposition to the ocean surface may also be important in controlling ozone concentration in the MIBL.

5. Individual layer structure and evolution

5.1. Marine internal boundary layer (MIBL) structure and evolution

5.1.1. Sea surface temperature. Fig. 8 shows the C-130 sea surface temperature (SST) measure-

Table 3. *Dominant soluble aerosol composition during Lagrangian 3 for fine-mode aerosol (<1.4 µm diameter)*

Flight, run	z (m)	$[NH_4^+]$ (ppt)	$[SO_4^{2-}]$ (ppt)	$[Cl^-]$ (ppt)	$[NO_3^-]$ (ppt)	$[NH_4^+]/[SO_4^{2-}]$
		1st flight — 1200–1500 UTC 23 July				
MIBL	120	2192	1039	77	63	2.1
PL	530	1638	809	150	87	2.0
PL	1040	1238	564	45	66	2.2
DL	1600	—	—	—	—	—
UPL	1950	2064	1632	204	27	1.3
		2nd flight — 2300 UTC 23 July–0200 UTC 24 July				
MIBL	250	2070	878	233	49	2.4
MIBL	530	1489	623	184	41	2.4
MIBL	870	1200	550	220	47	2.2
PL	1370	2077	943	40	19	2.2
FT	2020	521	271	<30	68	1.9
		3rd flight — 1200–1500 UTC 24 July				
MIBL	120	1523	758	222	42	2.0
MIBL	770	1385	636	49	28	2.2
MIBL	930	1349	844	70	9	1.6
PL	1120	—	—	—	—	—
FT	1860	115	39	<30	<5	2.9

Concentrations are expressed in ppt molar mixing ratio (i.e. moles of species per 10^{12} moles of air). The final column shows the molar ratio of ammonium to sulphate, which would be equal to 2 if the aerosol were composed entirely of ammonium sulphate $(NH_4)_2SO_4$.

Table 4. *Dominant soluble aerosol composition during Lagrangian 3 for large aerosol (>1.4 µm diameter)*

Flight, run	z (m)	$[Na^+]$ (ppt)	$[NH_4^+]$ (ppt)	$[SO_4^{2-}]$ (ppt)	$[Cl^-]$ (ppt)	$[NO_3^-]$ (ppt)
		1st flight — 1200–1500 UTC 23 July				
MIBL	120	954	<20	146	613	189
PL	530	<80	<20	61	20	<10
PL	1040	<80	<20	39	41	<10
DL	1600	—	—	—	—	—
UPL	1950	<80	162	279	<25	39
		2nd flight —— 2300 UTC 23 July–0200 UTC 24 July				
MIBL	250	783	<20	150	479	265
MIBL	530	566	<20	129	299	143
MIBL	870	242	<20	86	92	96
PL	1370	<70	51	117	<20	42
FT	2020	<90	<30	46	<25	<10
		3rd flight — 1200–1500 UTC 24 July				
MIBL	120	825	<20	126	513	237
MIBL	770	665	<20	137	360	91
MIBL	930	92	<20	114	20	72
PL	1120	—	—	—	—	—
FT	1860	<80	<30	<12	<23	<10

Concentrations are expressed in ppt molar mixing ratio (i.e. moles of species per 10^{12} moles of air).

Table 5. *Non-methane hydrocarbon measurements during Lagrangian 3*

	A566			A567			A568		
	[MIBL	PL	UPL]	[MIBL	PL	FT]	[MIBL	PL	FT]
ethane	0.629	0.953	0.718	0.699	0.851	0.737	0.721	0.736	0.728
propane	0.095	0.276	0.171	0.129	0.167	0.065	0.128	0.168	0.070
n-butane	0.031	0.067	0.060	0.034	0.048	0.010	0.030	0.030	0.009
isobutane	0.018	0.039	0.037	0.019	0.020	0.005	0.018	0.024	0.005
n-pentane	0.006	0.017	0.019	0.015	0.030	0.009	0.014	0.030	0.008
2-methylbutane	0.007	0.024	0.015	0.011	0.012	0.003	0.013	0.037	0.002
acetylene	0.113	0.195	0.193	0.125	0.144	0.039	0.135	0.118	0.044
benzene	0.052	0.058	0.059	0.041	0.039	0.009	0.044	0.068	0.014
toluene	0.008	0.017	0.011	0.009	0.028	0.011	0.013	0.032	0.012

Concentrations are expressed in parts per billion by volume. Values are given for the marine internal boundary layer (MIBL) the polluted layer (PL) and free troposphere (FT). Free tropospheric measurements were not available from A566. Instead, values in the upper polluted layer (UPL) are shown.
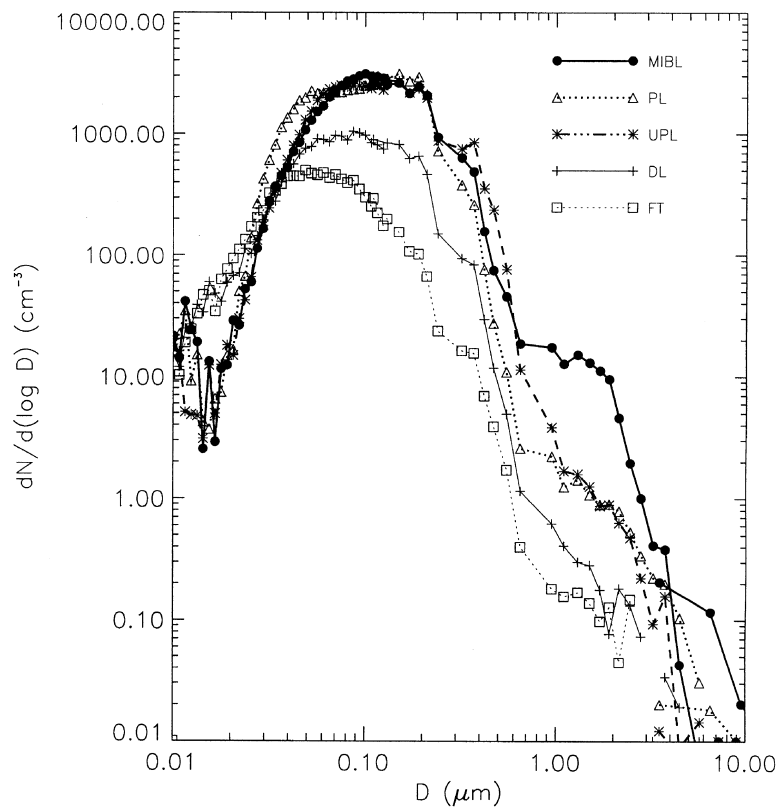

Fig. 6. Aerosol spectra from the 1st flight (A566) during Lagrangian 3. Spectra are shown from 5 heights.

ments obtained from the lowest aircraft legs together with the SST measured by the ship at the time of the release of the smart balloon. The dashed line is the ECMWF analysis sea surface temperature. It is clear that considerable discrepancy exists between the three observational datasets. While both the C-130 and AVHRR datasets show increasing SST the gradient of the increase
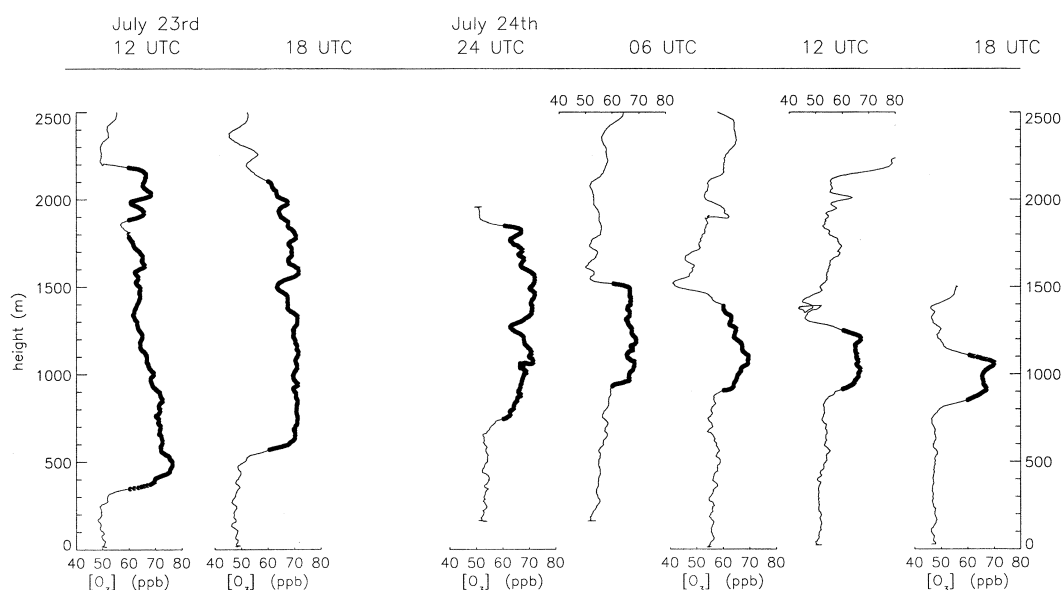
Fig. 7. Profiles of ozone concentration from Lagrangian 3. The approximate time of the profiles is shown at the top. Ozone concentrations greater than 60 ppb (by volume) are highlighted to show that ozone concentrations are highest in the polluted layer where the relative humidity is significantly lower (40–60%) than in the MIBL (80–100%).
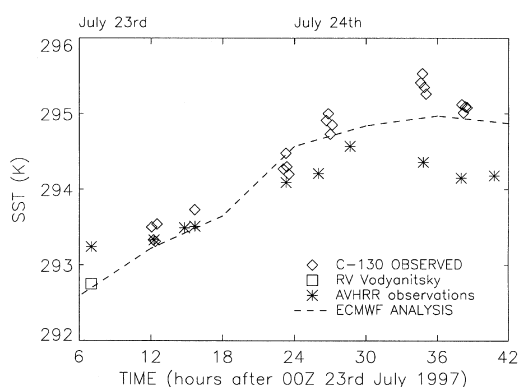

Fig. 8. Sea surface temperature measurements from Lagrangian 3. Shown on the graph are C-130 measurements (diamonds), AVHRR measurements (asterisks) and a ship measurement from the RV *Vodyanitskiy* (square). The dashed line shows the ECMWF analysis sea surface temperature. AVHRR SST retrievals (Vazquez et al., 1998) are taken from a 5-day average dataset (20–24 July).

is considerably more marked for the C-130 data. The C-130 SST data, which are believed to be more reliable than AVHRR agree very well with the ECMWF analysis SST which show a similar

increase followed by a levelling-off (and even a small decrease) towards the end of the observation period.

5.1.2. Thermodynamics and dynamics. Fig. 9 shows vertical wind variance from the three flights. The variance clearly shows that the MIBL was much more turbulent than the polluted layer above, where the variance is comparable to that found in the free troposphere. In the MIBL the latent and sensible heat fluxes (not shown) were positive indicating upward transport of heat and moisture.

The surface air temperature (extrapolated from the lowest level run down to 10 m using the dry adiabatic lapse rate) increases throughout the observational period from 292.7 K to 294.8 K in 30 h. The air temperature is consistently lower than the sea-surface temperature which results in vertical heat transport via convective overturning. Eddy-correlated and bulk thermodynamically-derived (Garratt, 1977; Bretherton et al., 1995) surface (10 m) sensible and latent heat fluxes agree to within the experimental sampling error (Lenschow et al., 1980). Surface latent heat fluxes

were much larger than the sensible heat fluxes throughout ($70–100\ \mathrm{W\ m^{-2}}$ and $4–6\ \mathrm{W\ m^{-2}}$ respectively) with a general increasing trend throughout the observational period.

The Monin–Obukhov length L_{MO} relates the relative importance of surface wind shear and convection in driving the boundary layer turbulence. In convective conditions L_{MO} is negative and has a magnitude that decreases with increasing importance of convective turbulence. During the observational period L_{MO} is consistently negative and has the smallest values ($L_{MO} \approx -150\ \mathrm{m}$) during the 2nd flight where the MIBL grew rapidly. Considerably larger values were observed during the 1st ($L_{MO} \approx -300\ \mathrm{m}$) and last ($L_{MO} \approx -350$ to $-700\ \mathrm{m}$) flights. This suggests that a possible cause of the rapid boundary layer growth may have been related to increasing convective turbulence during the 2nd flight. However, cloud-free turbulence is unlikely to have been sufficient to explain the rapid boundary layer growth. Previous studies of (Deardorff et al., 1980; Sullivan et al., 1998) have shown that the sensible heat flux at the inversion is an approximately constant fraction (0.1–0.2) of the surface sensible heat flux. As is shown in Solazzo et al. (2000) the surface sensible heat flux observed during Lagrangian 3 is far too small to generate the entrainment rates necessary to cause the rapid deepening of the MIBL during the 2nd flight. Cumulus clouds were forming at the top of

the MIBL during the period of rapid boundary layer growth and it is likely that these clouds served to produce higher entrainment rates through enhanced turbulence close to the MIBL inversion. The cumulus clouds were observed to penetrate the MIBL inversion in places and this served to moisten the layer immediately above the inversion. Johnson et al. (2000) shows that the MIBL inversion during Lagrangian 3 was unstable according to the cloud-top entrainment instability (CTEI) criterion of MacVean and Mason (1990) (pertaining to cases where the boundary layer is saturated and the layer above is subsaturated). This suggests that cumulus clouds impinging upon the MIBL inversion might have been able to cause rapid entrainment and thus boundary layer deepening. Further discussion on CTEI is found in Deardorff (1980) and Randall (1980).

5.1.3. Aerosol and chemical evolution. Fig. 10 shows that the MIBL aerosol size distribution across the entire size range remained almost unchanged during the observational period despite the rapid changes in MIBL depth. This is due to the fact that air entrained into the MIBL from the PL above had a similar aerosol spectrum (Fig. 6). Had the air above the MIBL been of free tropospheric nature the resulting dilution during the observational period would have reduced the MIBL total aerosol concentrations by some
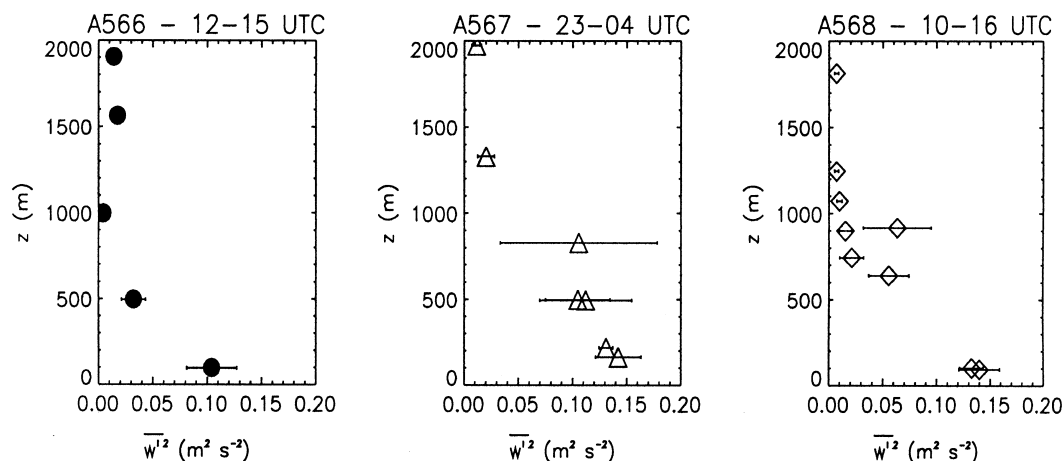

Fig. 9. Vertical wind variance from straight and level runs during Lagrangian 3. Each point represents the mean value for each box pattern.
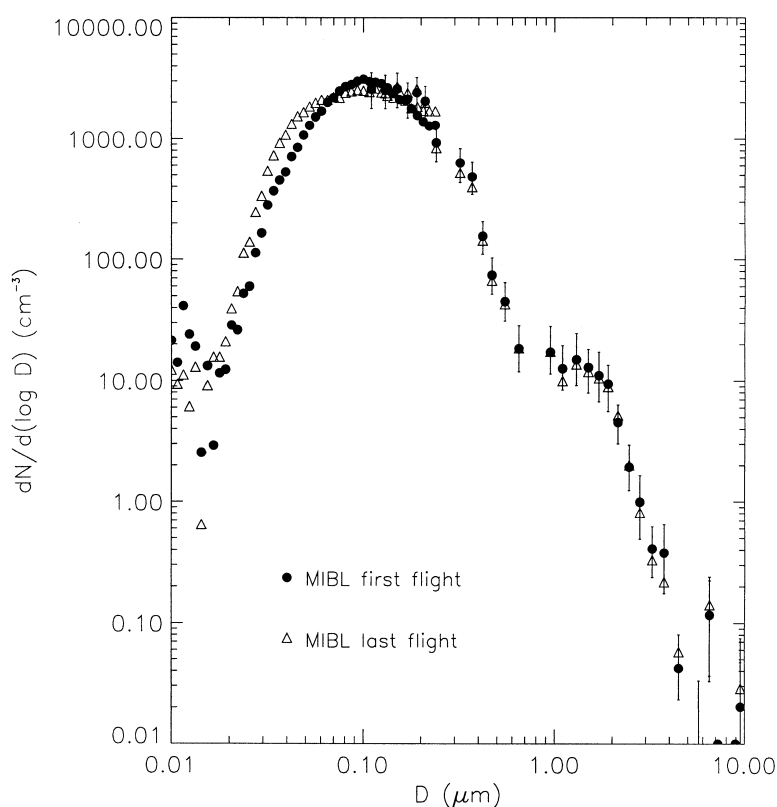
Fig. 10. Aerosol spectra from the marine internal boundary layer during the final flight (A568, triangles). The circles represent the boundary layer spectra from the 1st flight (A566) which shows that there was no substantial change in the aerosol spectrum in the MIBL during the observational period.

40–50% over the observational period. As Table 2 shows, the total aerosol number concentration remains unchanged throughout. There is a small decrease in the accumulation mode aerosol concentration in the MIBL from approximately $1000 \, cm^{-3}$ to below $900 \, cm^{-3}$ (10–15%), which coincides with a decrease in sulphate and ammonium mass in the fine-mode of approximately 30%. The size-distributions on the 1st and last flight (Fig. 10) do show a slight reduction in most accumulation mode size classes but the considerable horizontal variability (represented by the error bars) in the accumulation mode makes difficult any quantitative assessment of the change in accumulation mode aerosol concentrations. The decrease may be a result of dry deposition (no precipitation was observed during Lagrangian 3) at the sea surface although there is considerable uncertainty surrounding the values of dry depos-

ition velocities for aerosol particles (Seinfeld and Pandis, 1996). Hoell et al. (2000) estimated an accumulation mode aerosol concentration loss of only $6 \, cm^{-3}$ over a 26-h period during the 2nd Lagrangian experiment of ACE-2 (Osborne et al., 2000). Accumulation mode aerosol concentrations in the 2nd Lagrangian experiment were comparable to those in this study. This result would suggest that dry deposition is insufficient to explain the observed losses in both number and mass in the accumulation mode.

The air in the MIBL passed over the Benelux countries which would account for the molar ammonium/sulphate ratios of approximately 2 in the fine mode. This suggests an abundance of ammonia in the source regions and it is known that intensive animal farming, particularly of pigs, leads to high ammonia production in the Benelux countries.

In the coarse mode nitrate mixing ratios in the

MIBL were considerably higher than in the polluted layer above the MIBL (Table 4). In high sea-salt conditions and large relative humidities (relatively large amounts of liquid water available for aqueous reactions) the conversion of nitric acid (HNO_3) to the particulate phase (nitrate) can occur much more readily than in low relative humidities and low amounts of sea salt. Thus, it is likely that the conversion of nitric acid to solid nitrate was occurring or had occurred prior to the start of Lagrangian 3.

5.1.4. Potential for CCN activation in the MIBL. In polluted air masses, in contrast to clean air masses, it is generally found that a significant fraction of the aerosol larger than around 0.1 μm is unable to act as cloud condensation nuclei (CCN) (Martin et al., 1994; Chuang et al., 2000). This is investigated in Lagrangian 3 using a CCN spectrometer fitted to the C-130. It is possible, assuming a chemical composition for the aerosol, to convert a dry aerosol number-size spectrum into a CCN spectrum (Martin et al., 1994; Covert et al., 1998; Ji and Shaw, 1998). Reduction of the Van't Hoff factor with increasing solution molality has been modelled using the corrections of Young and Warren (1992) but makes little difference to the calculated critical supersaturations except when the ratio of solute mass to solution mass is greater than 20%. Assuming the soluble material in the CCN to be entirely ammonium sulphate (the dominant soluble aerosol type by mass during Lagrangian 3), a dry aerosol particle of a given size will activate into a cloud droplet if the supersaturation exceeds a fixed amount determined using Kohler theory modified to account for an insoluble component.

Fig. 11 shows both the measured and modelled CCN spectra calculated from the dry aerosol size spectra for aerosol soluble mass fractions of 5%, 20%, 50% and 100% (no insoluble material at all). In all cases (except for supersaturations below 0.1% on the 5% and 20% soluble mass fraction curves) the calculated CCN number concentration exceeds the measured number concentration. For the case where 50% of the mass in each aerosol is soluble the calculated concentrations are close to twice those measured. Similar results were found during ACE-2 with data obtained on the Merlin and Pelican aircraft (Chuang et al., 2000; Snider and Brenguier et al., 2000) and with pol-

luted data from Cape Grim (Bigg, 1986). When only 5% of the total aerosol mass is assumed to be soluble the agreement between modelled and measured CCN concentrations is better apart from supersaturations below 0.2%. The need for such low soluble fractions is contrary to the ground-based results from Tenerife (Putaud et al., 2000) which suggest much larger soluble mass fractions. Further, measurements made on Tenerife during ACE-2 suggest that the majority of aerosol particles in pollution outbreaks were internally rather than externally mixed (Putaud et al., 2000). Hygroscopicity measurements were made on the RV Vodyanitsky at the start of Lagrangian 3 show that a single mode is present in the hygroscopicity growth distributions for 0.05, 0.1, 0.15 and 0.25 μm dry aerosol particles. The mean growth factor itself ranged from 1.38 for 0.05 μm particles to 1.44 for 0.25 μm particles, values typical for polluted air masses observed in ACE-1 (Covert et al., 1998). The unimodal nature of the hydroscopicity distribution suggests that the aerosol particles (at least in the 0.05–0.25 μm size range) are internally rather than externally mixed. The discrepancy between observed and modelled CCN spectra thus remains a particular problem in the studies of aerosol-cloud closure.

5.2. Pollution layer (PL) structure and evolution
5.2.1. Thermodynamics and dynamics. In the pollution layer (PL) above the MIBL the vertical wind variance (Fig. 9) and the sensible and latent heat fluxes (not shown) were close to zero throughout Lagrangian 3. The momentum flux (not shown) was close to zero for all levels above the MIBL implying that very little generation of TKE is occurring in the pollution layer above the MIBL. In addition, no cloud formed in the PL throughout the observational period. The lack of TKE generation in the PL implies that there is no significant source of energy available for entrainment of free tropospheric air into the PL and hence dilution of PL air.

5.2.2. Aerosol and chemical evolution. The pollution layer aerosol dry size distributions (Fig. 6) are similar to those in the MIBL but with a slightly smaller modal radius (i.e., distribution shifted to smaller sizes relative to that in the MIBL). Total aerosol concentrations in the PL (Table 2) are very similar to those in the BL.
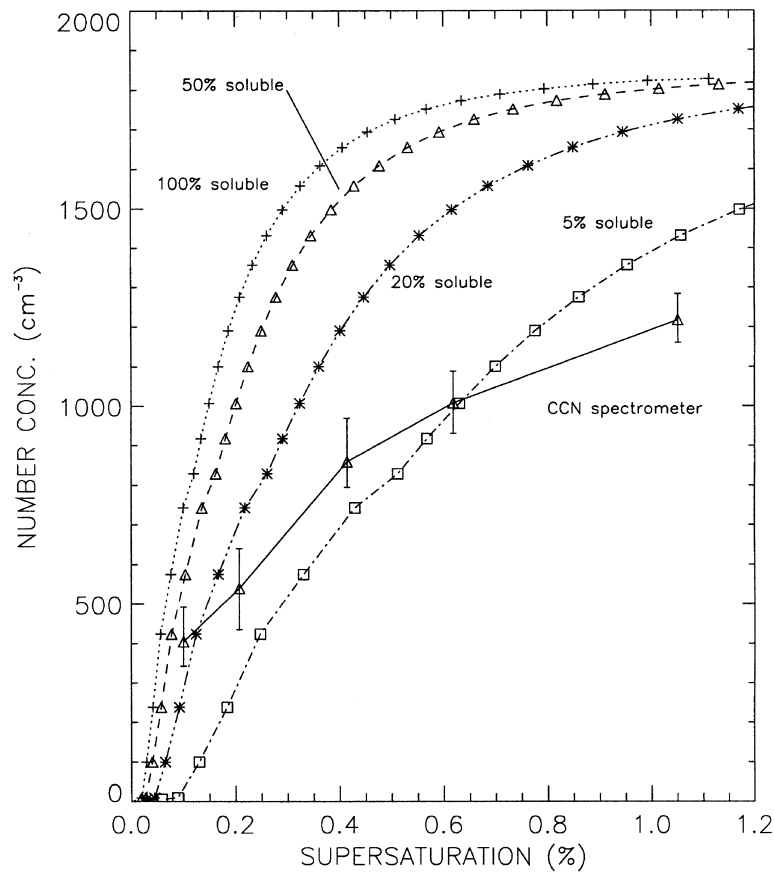
Fig. 11. Measured (triangles and solid line) and modelled CCN spectra from Lagrangian 3. The error bars represent the rms of the concentration from 4 individual spectra taken at a height of 120 m at the start of the 1st flight. Poor agreement between the spectra is observed if the aerosol are assumed to be fully soluble (crosses and dotted line).

Accumulation mode aerosol concentrations are also similar but the PL aerosol contains fewer particles larger than 0.25 μm and more in the size range 0.1–0.25 μm. This may be a reflection of cloud-processing prior to the start of the observational period, although the absence of a clear Hoppel dip in any of the spectra suggests that any cloud-processing had taken place a number of hours prior to the measurement period (Fitzgerald et al., 1998). Certainly, little cloud processing of aerosol can have taken place through in-cloud oxidation during the observational period as sulphur dioxide concentrations in the MIBL were close to clean marine background values. Little cloud processing can have taken place through coalescence during Lagrangian 3 because the

clouds were generally sparse with low liquid water contents. The coarse mode aerosol concentrations are greatly reduced in the PL suggesting that this air had little influence with the sea surface since leaving land.

Fine-mode sulphate and ammonium ionic concentrations are also lower in the PL than in the MIBL (Table 3) at the start of the observational period, although the molar ratio of ammonium to sulphate is close to 2 for both the PL and MIBL aerosol suggesting that the aerosol in composed predominantly of ammonium sulphate with little acidic bisulphate present. Back-trajectories suggest that the PL and MIBL layers had similar origins. Prior to the start of the observations cloud-processing could have raised the mass of sulphate in

the MIBL aerosol resulting in the depressed values in the PL at the start of the observational period. Evidence for a lack of cloud processing in the PL is found in the higher PL sulphur dioxide concentrations (60–100 ppt, compared with 15–30 ppt in the MIBL).

5.3. Dry layer (DL) structure and evolution

5.3.1. Thermodynamics and dynamics. The dry layer (DL, Fig. 4) situated between the two polluted layers was only observed on the 1st flight and at the start of the 2nd flight. The DL had low humidity (1–2 g kg^{-1}) characteristic of free tropospheric air. At 1200 UTC, the DL extended from 1550–1900 m altitude and subsided until its extent was from around 1050–1300 m. The thickness of the DL was variable (Fig. 3) with a thickness between 50 m and 350 m, which may be attributed to horizontal heterogeneity of the layer. That the DL was not observed after 0000 UTC 24 July could be a result of differential advection between the MIBL (the layer being tracked by the balloon) and higher levels. The vertical wind variance in the DL was small indicating that the propensity for mixing with layers above and below was small.

5.3.2. Aerosol and chemical evolution. The DL was relatively clean ($N_{tot} = 600$–700 cm^{-3}) although these values are around twice that of the free troposphere observed during Lagrangian 3. The origin of the DL is not clear, although the back-trajectories give a suggestion: the trajectory which at the start of the observational period was at a height of 1500 m was, 4 days before, at a greater altitude than any of the other trajectories. This suggests that the DL had continental free tropospheric origins rather than convective boundary layer origins. Some mixing with polluted air may have taken place after leaving the continent. No filter measurements were made exclusively in the DL and so no chemical analysis is available.

5.4. Upper polluted layer (UPL) structure and evolution

5.4.1. Thermodynamics and dynamics. The upper polluted layer (UPL) was a layer of specific humidity (5–7 g kg^{-1}) intermediate between that of the MIBL and the free troposphere. The relative humidity in the UPL was 55–75%. Turbulence levels were small indicating little mixing with either the free troposphere or the layers below. The UPL was only observed on the 1st flight and it is unlikely that its identity was lost due to mixing. More likely, differential advection (wind speed/direction in the UPL was 8 m s^{-1} as opposed to 10 m s^{-1} in the MIBL) was the cause of the loss of the UPL — the differential advection between the MIBL and the UPL would have shifted a point in the UPL by nearly 100 km in 12 h.

5.4.2. Aerosol and chemical evolution. Fig. 6 shows that the dry size distribution of aerosol in the UPL is somewhat broader than in the PL and MIBL with significantly higher concentrations in the size range 0.4–1.0 μm. Total aerosol concentrations in the UPL ($N_{tot} = 2000$–2300 cm^{-3}) were slightly higher than in the PL and MIBL as were the accumulation mode concentrations. The most interesting features of the aerosol in the UPL however is the chemical compostion, which suggests remarkably different origins for the air in this layer. In the fine mode, the molar ratio of ammonium to sulphate was 1.3 (Table 3), significantly lower than that in the MIBL and PL (close to 2), and indicative of more acidic aerosol. In addition, considerable quantities of chloride was present in the fine mode, which due to the altitude of the UPL, is unlikely to have originated as sea-salt. High amounts of chloride have been linked (Tomsa et al., 1982) to output from coal-fired power stations. Back-trajectories for air at the start of Lagrangian 3 suggest that the layer at 2000 m (the observed UPL) can be traced back to the United Kingdom where coal-fired power stations are prevalent. This would also account for the lower ammonium/sulphate ratios in the UPL. Fossil fuel burning results in acidic aerosol which suggests that the UPL aerosol may have contained ammonium bisulphate as well as ammonium sulphate.

5.5. Free troposphere (FT) structure and evolution

The free troposphere was characterised by low humidities (<4 g kg^{-1}) and low aerosol concentrations ($N_{tot} = 300$–400 cm^{-3}; $N_{D > 0.1 \, \mu m} = 60$–$120$ cm^{-3}) throughout Lagrangian 3. The dominant soluble species in the fine mode were ammonium and sulphate, with some nitrate observed on one of the FT filter samples. Aerosol

spectra from the FT (Fig. 6) show much lower concentrations than in all other layers for diameters greater than 0.04 μm. For diameters smaller than this the FT concentrations were larger than those in the polluted layers and comparable to those in the DL.

6. Discussion

Detailed observations of the Lagrangian evolution of a lower tropospheric air mass advected from continental Europe were made using the UK Meteorological Office C-130 aircraft. Three flights over a 30-h period were carried out, the locations of which were determined by tracking a smart balloon launched from the research ship *Vodyanitsky*.

Observations at the start of the experiment showed polluted layers up to a height of 2000 m. Within the pollution layer a convective marine internal boundary layer (MIBL) was present. The pollution layer above the MIBL contained relatively low levels of turbulence. During the course of the observations the top of the pollution layer lowered due to subsidence in the lower troposphere. The MIBL grew during the observational period from around 500 m to 900–1000 m. Most of the MIBL growth occurred during the night between 2400 UTC 23 July and 0600 UTC 24 July and was associated with an increase in the cumulus cloud activity during this period. Cloud-top entrainment instability at the top of the cumulus clouds is a possible mechanism for the large entrainment rates necessary to cause such rapid MIBL growth.

Back trajectories from the start of the observational period showed that the air mass below 1500 m had passed over highly polluted areas of Europe including The Netherlands and Belgium. Some evidence shows that the pollution in the thin polluted layer above 1500 m probably passed over the UK. Chemical analysis of the aerosol in the different layers showed that the most important soluble ionic species in the polluted air were ammonium and sulphate. The molar ratio of ammonium/sulphate was close to 2.0 in the air below 1500 m and only 1.3 in the upper pollution layer suggesting that the lower pollution layer aerosol was less acidic than that in the upper pollution layer. This is consistent with high levels of ammonia release in the intensive animal farming regions of The Netherlands and Belgium.

Aerosol spectra during Lagrangian 3 were characterised by a single broad mode centered on 0.1 μm. The aerosol was fairly aged having traversed a sea-track for 2 days. Sulphur dioxide gas concentrations were significantly lower than during the 2nd Lagrangian experiment (Osborne et al., 2000) suggesting that most of the gas-to-particle conversion had taken place prior to the observational period. The potential for the aerosol to act as CCN was studied by direct measurement of the CCN supersaturation spectrum and by calculating the CCN spectrum from the PCASP/DMA dry aerosol size spectrum using a soluble mass fraction and the assumption that the soluble mass fraction is the same for each aerosol size. There was marked discrepancy between the measured and modelled CCN spectrum with the predicted CCN concentrations exceeding those measured in the supersaturation range 0.1–1.0%.

Aerosol spectra in the MIBL showed practically no changes over the observational period. Aerosol spectra above the MIBL in the polluted layer were similar to those in the MIBL. Thus, entrainment of air into the MIBL does not have a diluting effect in this case. The polluted layer, initially with a cap at a height of over 2000 m, became shallower during the observational period due to subsidence above the MIBL. At the end of the observational period a polluted layer between the free troposphere and the MIBL still existed but had become much thinner (250 m). Aerosol concentrations in the turbulent boundary layer over the ocean can only become affected by entrainment when subsidence has reduced the depth of the polluted layer (which may well be three to four times the height of the MIBL a short distance from land) so that no intermediate polluted layer exists between the turbulent boundary layer and the free troposphere. In Lagrangian 3 observations and back-trajectories show that the time taken for this to occur was at least 3.5 days. Clearly, differential advection is important in determining the vertical structure of pollution outbreaks and therefore the rate of transition from a polluted continental to a clean marine boundary layer. In the case presented here there was relatively little differential advection during the transport of the aerosol from its continental origin to the observational location (lowest 4 levels in Fig. 1). In other cases, pollution layers

above the developing MIBL may be advected away and replaced with clean air which would increase the rate at which MIBL air becomes diluted by entrainment.

7. Hypotheses

We have formulated five hypotheses from the observations which represent the most important findings from this study. It is intended that the hypotheses can be validated or refuted with future modelling studies.

- The processes affecting the aerosol size spectrum are in "pseudo-equilibrium" resulting in an unchanging spectrum.
- The processes affecting the aerosol size spectrum are acting on time scales much longer than the 30 h and so no changes in spectral shape could be observed.
- Cloud-topped BLs will lead to a significantly faster evolution from a continental to a marine air mass than cloud-free BLs due to enhanced entrainment rates.
- The time scale of the transition from a continental to a marine boundary layer is dependent upon the rate of horizontal differential advection of the residual continental pollution above the developing MIBL.
- Aerosol in polluted air masses is not fully soluble and thus its CCN properties cannot be determined by the assumption of complete aerosol solubility.

The 1st two hypotheses reflect the observational finding that no significant change was observed in the aerosol spectrum throughout the observational period. Entrainment of free tropospheric air

into the MIBL is enhanced by clouds and the 3rd hypothesis could thus be tested using combined boundary layer and aerosol models. The fourth hypothesis could be tested using transport models. The final hypothesis reflects the discrepancy between measured and modelled CCN spectra. It is hoped that the Lagrangian 3 dataset presented here will be useful in the development and validation of continental outbreak models.

8. Acknowledgements

REFERENCES

Andreae, M. O., Berresheim, H., Andreae, T. W. Kritz, M. A., Bates, T. S. and Merrill, J. T. 1988. Vertical distribution of dimethylsulfide, sulfur dioxide, aerosol ions, and radon over the northeast pacific ocean. *J. Atmos. Chem.* **6**, 149–173.

Bates, T. S., Kapustin, V. N., Quinn, P. K., Covert, D. S., Coffman, D. J., Mari, C., Durkee, P. A., DeBruyn, W. J. and Saltzmann, E. S. 1998. Processes controlling the distribution of aerosol particles in the marine boundary layer during ACE-1. *J. Geophys. Res.* **103**(D13) 16369–16383.

Bigg, E. K. 1986. Discrepancy between observation and

prediction of cloud condensation nuclei. *Atmos. Res.* **20**, 8–86.

Bretherton, C. S., Austin, P. and Siems, S. T. 1995. Cloudiness and marine boundary layer dynamics in the astex Lagrangian experiments (II) Cloudiness, drizzle, surface fluxes and entrainment. *J. Atmos. Sci.* **52**, 2724–2735.

Brooks, I. M. and Rogers, D. P. 1997. Aircraft observations of boundary layer rolls off the coast of California. *J. Atmos. Sci.* **54**, 1834–1849.

Businger, S., Johnson, R., Katzfey, J., Siems, S. and Wang, Q. 1999. Smart tetroons for Lagrangian air-mass

tracking during ACE-1. *J. Geophys. Res.* **104**, D9, 11709–11722.

Chuang, P. Y., Collins, D. R., Pawloska, H., Snider, J. R., Jonsson, H. H., Brenguier, J. L., Flagan, R. C. and Seinfeld, J. H. 2000. CCN measurements during ACE-2 and their relationship to cloud microphysical properties. *Tellus* **52B**, 843–867.

Covert, D. S., Gras, J. L., Wiedensohler, A. and Stratmann, F. 1998. Comparison of directly measured CCN with CCN modeled from the number-size distribution in the marine boundary layer during ACE-1 at Cape Grim, Tasmania. *J. Geophys. Res.* **103** (D13), 16597–16608.

Deardorff, J. W. 1980. Cloud top entrainment instability. *J. Atmos. Sci.* **37**, 561–563.

Deardorff, J. W., Willis, G. E. and Stockton, B. H. 1980. Laboratory studies of the entrainment zone of a convectively mixed layer. *J. Fluid Mech.* **100**, 41–64.

Draxler, R. R. and Hess, G. D. 1997. *Description of the hysplit 4 modelling.* Technical Memorandum ERL ARL-224, NOAA.

Fitzgerald, J. W., Marti, J. J., Hoppel, W. A., Frick, G. M. and Gelbard, F. 1998. A one-dimensional sectional model to simulate multicomponent aerosol dynamics in the marine boundary layer: 2. Model application. *J. Geophys. Res.* **103** (D13), 16103–16117.

Garratt, 1977. Review of drag coefficients over oceans and continents. *Mon. Wea. Rev.* **105**, 915–929.

Garvey, D. M. and Pinnick, R. G. 1983. Response characteristics of the particle measuring systems active scattering aerosol spectrometer probe (ASASP-X). *Aero. Sci. Technol.* **2**, 477–488.

Hignett, P. 1998. *Notes on correction of airborne sea surface temperature measurements for non-blackness effects.* Internal Note 28, Meteorological Research Flight.

Hoell, C., O'Dowd, C., Osborne, S. R. and Johnson, D. W. 2000. Timescale analysis of marine boundary layer aerosol evolution: Lagrangian case studies under clean and polluted conditions. *Tellus* **52B**, 423–438.

Ji, Q. and Shaw, G. E. 1998. On supersaturation spectrum and size distributions of cloud condensation nuclei. *Geophys. Res. Lett.* **25**, 1903–1906.

Johnson, D. W. et al. 2000. Overview of the Lagrangian experiments undertaken during the north Atlantic regional aerosol characterisation experiment (ACE-2). *Tellus* **52B**, 290–320.

Johnson, R., Businger, S. and Baerman, A. 2000. Lagrangian air mass tracking with smart balloons during ACE-2. *Tellus* **52B**, 321–334.

Lenschow, D. H., Wyngaard, J. C. and Pennell, W. T. 1980. Mean-field and second-moment budgets in a baroclinic, convective boundary layer. *J. Atmos. Sci.* **37**, 1313–1326.

MacVean, M. K. and Mason, P. J. 1990. Cloud-top entrainment instability through small-scale mixing and its parameterization in numerical models. *J. Atmos. Sci.* **47**, 1012–1030.

Martin, G. M., Johnson, D. W. and Spice, A. 1994. The

measurement and parameterization of effective radius of droplets in warm stratocumulus clouds. *J. Atmos. Sci.* **51**, 1823–1842.

Masuda, K., Takashima, T. and Takayama, Y. 1988. Emissivity of pure and sea waters for the model sea surface in the infrared window regions. *Remote Sensing of Environ.* **24**, 313–329.

Osborne, S. R., Johnson, D. W., Wood, R., Bandy, B., Andreae, M. O., O'Dowd, C., Glantz, P., Noone, K., Rudolph, J., Bates, T. S. and Quinn, P. K. 2000. Evolution of the aerosol, cloud and boundary layer dynamic and thermodynamic characteristics during the second lagrangian experiment of ACE-2. *Tellus* **52B**, 375–400.

World Climate Program 1986. *A preliminary cloudless standard atmosphere for radiation computation,* World Meteorol. Organ., Geneva.

Pueschel, R. F., Overbeck, V. R., Snetsinger, K. G., Russell, P. B., Ferry, G. V., Wilson, J. C., Livingston, J. M., Verma, S. and Fong, W. 1990. Calibration correction of an active scattering spectrometer probe to account for refractive index of stratospheric aerosols. *Aero. Sci. Technol* **12**, 992–1002.

Putaud, J. P., Van Dingenen, R., Mangoni, M., Virkkula, A., Raes, F., Maring, H., Prospero, J. M., Swietlicki, E., Berg, O. H., Hillamo, R. and Makela, T. 2000. Chemical mass closure and origin assessment of the submicron aerosol in the marine boundary layer and the free troposphere at Tenerife during ACE-2. *Tellus* **52B**, 141–168.

Raes, F., S. Bates, T., McGovern, F. and Van Liederkerke, M. 2000. The second aerosol characterisation experiment (ACE-2): general overview and main results. *Tellus* **52B**, 111–126.

Randall, D. A. 1980. Conditional instability of the first kind upside down. *J. Atmos. Sci.* **37**, 125–130.

Russell, L. M., Lenschow, D. H., Laursen, K. K., Krummel, P. B., Siems, S. T., Bandy, A. R., Thornton, D. C. and Bates, T. S. 1988. Bidirectional mixing in an ace 1 marine boundary layer overlain by a second turbulent layer. *J. Geophys. Res.* **103** (D13), 16411–16432.

Seinfeld, J. H. and Pandis, S. N. 1996. *Atmospheric chemistry and physics.* John Wiley and Sons, Toronto, Canada.

Snider, J. and Brenguier, J. L. 2000. Cloud condensation nuclei and cloud droplet measurements during ACE-2 *Tellus* **52B**, 828–842.

Solazzo, M. J., Russell, L. M., Percival, D., Osborne, S., Wood, R. and Johnson, D. W. 2000. Entrainment rates during ACE-2 Lagrangian experiments calculated from aircraft measurements. *Tellus* **52B**, 335–347.

Stull, R. B. 1988. *Boundary layer meteorology.* Kluwer Academic Publishers.

Sullivan, P. P., Moeng, C.-H., Stevens, B., Lenschow, D. H. and Mayor, S. D. 1998. Structure of the entrainment zone capping the convective atmospheric boundary layer. *J. Atmos. Sci.* **55**, 3042–3064.

Tomasa, U., Maenhaut, W. and Cafmeyer, J. 1982. Trace elements in atmospheric aerosols at Katowice, Poland.

In *Trace substances in environmental health.* ISBN pp 102–115.

Van Dingenen, R., Raes, F., Putaud, J-P., Virkkula, A. and Mangoni, M. 1999. Processes determining the relationship between aerosol number and non-sea-salt sulphate mass concentrations in the clean and perturbed marine boundary layer. *J. Geophys. Res.* **104**, 8027–8038.

Vazquez, J., Perry, K. and Kilpatrick, K. 1998. NOAA/ NASA AVHRR oceans pathfinder sea surface temperature data set user's reference manual. *Technical Report D-14070.* Jet Propulsion Laboratory.

Wang, S. C. and Flagan, R. C. 1990. Scanning electrical particle sizer. *Aer. Sci. and Tech.* **13**, 230–249.

Young, K. C. and Warren, A. J. 1992. A reexamination of the derivation of the equilibrium supersaturation curve for soluble particles. *J. Atmos. Sci.* **49**, 1138–1143.